

# ChemComm

Accepted Manuscript



This article can be cited before page numbers have been issued, to do this please use: Q. Zhou, B. Xin, Y. Wang, C. Li, Z. Chen, Q. Yu, Z. Huang and M. Zhu, *Chem. Commun.*, 2018, DOI: 10.1039/C8CC00533H.



This is an Accepted Manuscript, which has been through the Royal Society of Chemistry peer review process and has been accepted for publication.

Accepted Manuscripts are published online shortly after acceptance, before technical editing, formatting and proof reading. Using this free service, authors can make their results available to the community, in citable form, before we publish the edited article. We will replace this Accepted Manuscript with the edited and formatted Advance Article as soon as it is available.

You can find more information about Accepted Manuscripts in the [author guidelines](#).

Please note that technical editing may introduce minor changes to the text and/or graphics, which may alter content. The journal's standard [Terms & Conditions](#) and the ethical guidelines, outlined in our [author and reviewer resource centre](#), still apply. In no event shall the Royal Society of Chemistry be held responsible for any errors or omissions in this Accepted Manuscript or any consequences arising from the use of any information it contains.

Journal Name

COMMUNICATION

## Geminal cross-coupling synthesis, ion-induced emission and lysosome imaging of cationic tetraarylethene oligoelectrolytes

 Qi-Yuan Zhou,<sup>#</sup> Bo Xin,<sup>#</sup> Ya-Long Wang,<sup>#</sup> Chong Li,<sup>\*</sup> Ze-Qiang Chen, Qi Yu, Zhen-Li Huang, and Ming-Qiang Zhu<sup>\*</sup>

 Received 00th January 20xx,  
Accepted 00th January 20xx

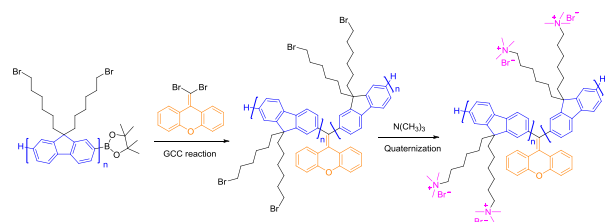
DOI: 10.1039/x0xx00000x

www.rsc.org/

Neutral conjugated tetraarylethene  $OF_n$  ( $n = 1-3$ ) and corresponding cationic conjugated oligoelectrolytes  $OF_{n+}$  ( $n = 1-3$ ) with aggregating-induced emission activity have been designed and synthesized using geminal cross-coupling.  $OF_{n+}$  ( $n = 1-3$ ) exhibit featured ion-induced emission in aqueous solution. They are used for lysosomal fluorescence imaging and tracing of lysosome events.

Most conventional fluorophores suffer from aggregation caused quenching (ACQ), in which the fluorescence at solid state diminishes relative to that in dilute solution. The latter state represents isolated molecules and does not suffer from detrimental aggregation effects that can decrease the fluorescence quantum yields. Considering the fact that many applications of light-emitting materials are in the solid-state, *i.e.* OLEDs, the efficient ways to alleviate solid-state fluorescence quenching have become important research topics. One excellent example of this is aggregation induced emission (AIE)<sup>1-3</sup> whose solid-state fluorescence increases dramatically relative to its solution-state fluorescence. A phenomenon that is the exact opposite of ACQ was unexpected. The benefits from this strategy in improving fluorescence properties in the “aggregate” state have been exploited in several research areas, including OLEDs, sensors and bioimaging.<sup>4-6</sup> It is noteworthy that few reports on ionic AIE fluorogens in aqueous solution, which may be more beneficial in biosensors or bioimaging.<sup>7-9</sup>

One archetypal AIE-active material is tetraphenylethene (TPE) and has been extensively reported in the literatures due to its prominent AIE properties, high solid-state fluorescence quantum yields and ease of synthesis/modification.<sup>10-12</sup> Recently, we have reported intriguing AIE-active adducts and investigated the optical and photophysical properties.<sup>13,14</sup> We

Scheme 1 Synthetic route to  $OF_n$  and  $OF_{n+}$ .

have demonstrated remarkable fluorescence quenching in solution with enhanced emission in the “aggregate” state of an analogous series of fluorene oligomers end-capped with TPE.<sup>13</sup> It is concluded that as the length of central oligofluorene unit increases between the two end-capped TPE groups, the AIE-effect of the associated material gradually decreases, indicating that the TPE units have a reduced influence on the AIE-effect as the conjugation length increases.<sup>15</sup> On the basis of these results, here, a series of neutral conjugated fluorogens  $OF_n$  and corresponding cationic conjugated oligoelectrolytes  $OF_{n+}$  ( $n = 1-3$ , ‘O’ presents the 9-methylene-9H-xanthene as it has an oxygen bridge between two benzene rings, while ‘F<sub>n</sub>’ or ‘F<sub>n+</sub>’ represents the number of the Fluorene repeating unit at each side of ‘O’ segment, as shown in Scheme 1), where two oligofluorenes and one 9-methylene-9H-xanthene in each molecule construct a AIE-active tetraarylethene structure, have been designed and synthesized using geminal cross-coupling (GCC) reaction of 1,1-dibromoolefins with aryl boric acid ester.<sup>16</sup>

The synthetic procedures of the neutral conjugated fluorogens  $OF_n$  ( $n = 1-3$ ) and corresponding cationic conjugated oligoelectrolytes  $OF_{n+}$  ( $n = 1-3$ ) are shown in Scheme 1 and Scheme S1-S3. The neutral conjugated fluorogens  $OF_n$  ( $n = 1-3$ ) were synthesized by the standard palladium-mediated GCC between oligofluorenes borate derivatives  $F_n$  and 9-(dibromomethylene)-9H-xanthene with an isolated yield higher than 64%. The corresponding cationic conjugated oligoelectrolytes  $OF_{n+}$  were prepared through treatment of the precursor  $OF_n$  with trimethylamine in ethanol. The chemical structures of the neutral conjugated fluorogens

Wuhan National Laboratory for Optoelectronics, School of Optical and Electronic Information, Huazhong University of Science and Technology, Wuhan, 430074, Hubei, China, E-mail: mqzhu@hust.edu.cn, chongli@hust.edu.cn; Fax: +86-27-87793419.

<sup>†</sup> Electronic Supplementary Information (ESI) available: experimental procedures/characterization, optical spectra, and molecular simulation. See DOI: 10.1039/x0xx00000x

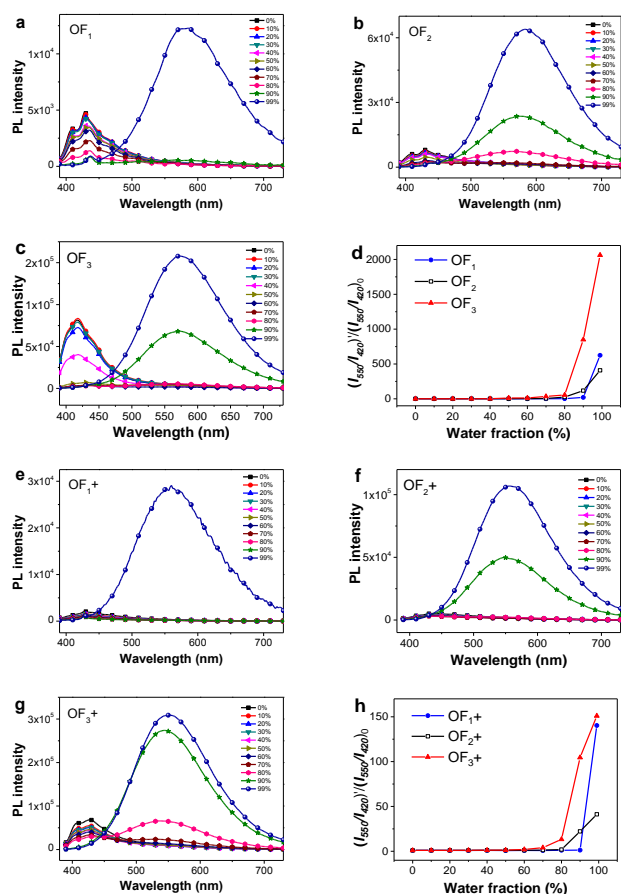


**Fig. 1** AIE effect of  $OF_n$  in water-THF and  $OF_{n+}$  in DMSO-THF binary solvents with various THF volume fractions. Fluorescence spectra of (a)  $OF_1$ , (b)  $OF_2$ , (c)  $OF_3$ , (e)  $OF_{1+}$ , (f)  $OF_{2+}$ , (g)  $OF_{3+}$ . The changes of normalized emission intensity ratio at 550 nm and 420 nm  $[I_{550}/I_{420}]/[I_{550}/I_{420}]_0$  versus water fractions of (d)  $OF_n$  and (h)  $OF_{n+}$ . The concentrations of  $OF_n$  and  $OF_{n+}$  are 2  $\mu M$ . The excitation wavelength is 380 nm.

$OF_n$  and corresponding cationic conjugated oligoelectrolytes  $OF_{n+}$  ( $n = 1-3$ ) were studied by  $^1H$  NMR spectra (Fig. S1). They were estimated to have high quaternization degree of 99.5%, 97.0% and 95.9%, respectively by calculating the ratio of the integrated area of the H atoms on Xanthone moiety (6.7 ppm) to that of  $-CH_2 N(CH_3)_3$  (3.0 ppm). Due to the high charge density, the cationic conjugated oligoelectrolytes  $OF_{n+}$  ( $n = 1-3$ ) exhibit good solubility in both aqueous media and highly polar organic solvents.

The normalized UV-vis absorption and photoluminescence (PL) spectra of  $OF_n$  ( $n = 1-3$ ) in THF or in water are depicted in Fig. S2. The absorbance of  $OF_n$  ( $n = 1-3$ ) at 344 nm (a shoulder peak), 345 nm, 360 nm are ascribed to the fluorene segments. Compared to  $OF_1$ , the maximum absorption peaks of  $OF_2$ ,  $OF_3$  red shift 31 nm and 46 nm which is attributed to the more  $\pi$ -conjugated fluorine units (Fig. S2a). The optimized molecular structures and HOMO /LUMO energy levels of  $OF_n$  are shown in Fig. S3. The HOMO and LUMO of  $OF_n$  are contributed by both the orbitals of TAE and oligofluorenes. The effective conjugation length becomes longer with increasing the length of oligofluorenes incorporating to the tetraarylethylene (TAE) segment. Through theoretical calculations, the energy bandgap  $E_g$  for  $OF_n$  ( $n = 1-3$ ) is 3.84 eV, 3.64 eV and 3.56 eV,

respectively, which is in consistency with their absorption wavelengths. The  $E_g$  becomes more and more narrow from  $OF_1$  to  $OF_3$ , which explains the successively absorption redshift of  $OF_n$  ( $n = 1-3$ ).  $OF_n$  ( $n = 1-3$ ) show blue emission in THF with the maximum emission peaks centered at 428 nm, 430 nm, 418 nm and yellow emission in water with the maximum emission peaks centered at 586 nm, 582 nm, 572 nm (Fig. S2b). The blue emission of  $OF_n$  ( $n = 1-3$ ) in THF is originated from the oligofluorenes while the yellow emission is attributed to TAE structure<sup>17</sup> where the oligo-fluorene segment has increased the conjugation length, which is not ascribed to keto defects or excimers in poly- and oligofluorenes.<sup>18</sup> (Fig. S4) Due to the ACQ feature of oligofluorenes, the blue emission peak of  $OF_n$  totally disappears when aggregated in water. It is noteworthy that the Stock shifts of  $OF_n$  at aggregated state are larger than 200 nm, which is beneficial to sensing and imaging applications.

$OF_n$  exhibit the complementary AIE and ACQ effect in THF-water binary solvents which is demonstrated by measuring the photoluminescence (PL) of  $OF_n$ .  $OF_n$  as hydrophobic luminogens can be easily dissolved in THF but perform aggregated state in water. The  $OF_n$  molecules aggregate to different extent in the different volume ratios of THF-water binary solvents. Fig. 1a-1c show the PL spectra of  $OF_n$  in THF-water mixtures with increasing water fraction. The PL intensity at around 420 nm decreases in high water fraction binary solvents while that of around 570 nm increases. The emission of around 570 nm remains weak until up to 80% of water is added to the THF solution. Nevertheless, it increases dramatically at 90% water content. Fig. 1d shows the plot of normalized fluorescence intensity ratio  $([I_{550}/I_{420}]/[I_{550}/I_{420}]_0)$  versus water fraction. The  $[I_{550}/I_{420}]/[I_{550}/I_{420}]_0$  of  $OF_3$  at 99% water content is 2062 which is 5 and 3 times as much as those of  $OF_2$  and  $OF_1$ , respectively. The relative quantum yield (QY) of  $OF_3$  is estimated to be 1.69% in THF and 35.85% in water relative to quinine sulfate (QY = 55% in 0.1 M  $H_2SO_4$ ) (Table S1), which are both higher than those of  $OF_2$  and  $OF_1$ . The transformation from blue emission to yellow emission of  $OF_3$  is more intense than those of  $OF_2$  and  $OF_1$  when aggregated in poor solvent. Hence, we draw a conclusion that  $OF_3$  exhibits the most distinctive ratiometric fluorescence response to a poor solvent.

We further investigate the AIE properties of organic quaternary ammonium  $OF_{n+}$  ( $n = 1-3$ ). As cationic compounds,  $OF_{n+}$  are well soluble in water and highly polar organic solvents like DMSO, methanol and ethanol but insoluble in low polar solvents such as THF. In particular,  $OF_{n+}$  ( $n = 1-3$ ) are better soluble in highly polar organic solvents (DMSO and methyl alcohol) than in water which is due to the amphiphilic character of  $OF_{n+}$  ( $n = 1-3$ ). Thus, we choose DMSO as the good solvent and THF as the poor solvent for the PL examination to investigate the AIE effect of  $OF_{n+}$  ( $n = 1-3$ ). As shown in Fig. 1e-1g, the blue emissions of  $OF_{n+}$  ( $n = 1-3$ ) in DMSO are not significant compared to their yellow emission in THF. With increasing the poor solvent fraction, the blue emission at around 430 nm decreases meanwhile the yellow emission at around 560 nm increases. The fluorescence color sensitivity to poor solvent than  $OF_{1+}$  and  $OF_{2+}$ . The relative

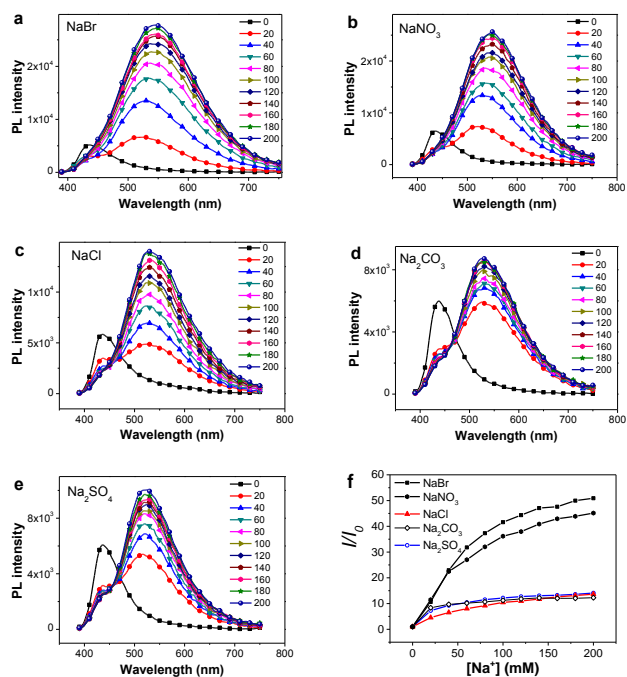


**Fig. 2** Fluorescence spectra of  $OF_1^+$  in aqueous solution of different sodium salt (concentration unit: mM). (a) NaBr, (b)  $NaNO_3$ , (c) NaCl, (d)  $Na_2CO_3$ , (e)  $Na_2SO_4$ . (f) The enhancement of emission peak intensity at 550 nm versus  $Na^+$  concentration  $[Na^+]$  with various anions. The concentration of  $OF_1^+$  is 2  $\mu M$ . The excitation wavelength is 380 nm.

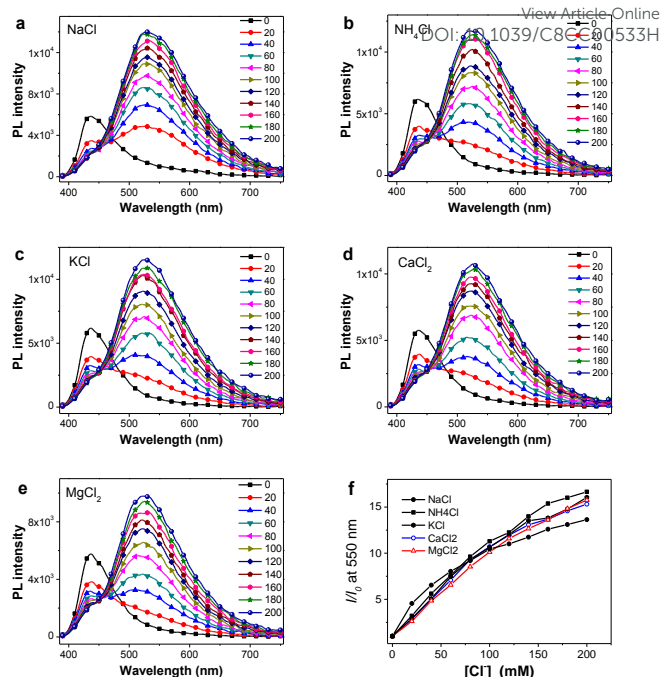


**Fig. 3** Fluorescence spectra of  $OF_1^+$  in aqueous solution of different chloride salt (concentration unit: mM). (a) NaCl, (b)  $NH_4Cl$ , (c) KCl, (d)  $CaCl_2$ , (e)  $MgCl_2$ . (f) The enhancement of emission peak intensity at 550 nm versus  $Cl^-$  concentration  $[Cl^-]$  with various cation. The concentration of  $OF_1^+$  is 2  $\mu M$ . The excitation wavelength is 380 nm.

QYs of  $OF_n^+$  ( $n = 1-3$ ) are estimated to be 2.89%, 2.09%, 4.20% sensitivity to poor solvent than  $OF_1^+$  and  $OF_2^+$ . The relative QYs of  $OF_n^+$  ( $n = 1-3$ ) are estimated to be 2.89%, 2.09%, 4.20% in DMSO and 29.95%, 32.85%, 38.62% in THF relative to quinine sulfate (QY = 55% in 0.1 M  $H_2SO_4$ ) (Table S1).

An interesting discovery for these hydrophilic cationic oligoelectrolytes is that  $OF_n^+$  ( $n = 1-3$ ) exhibit strong salt or ionic effect (Fig. S5 and Note S1). The emission spectra of organic quaternary aminated  $OF_1^+$  in aqueous solution of different sodium salts are measured (Fig. 2). As shown in Fig. 2a-2e, the blue emission of  $OF_1^+$  in water decreases significantly while its yellow emission increases abruptly along with ion concentration increasing. The emission enhancement of  $OF_1^+$  become stronger in the order of  $SO_4^{2-}$  (x 12),  $CO_3^{2-}$  (x 14),  $Cl^-$  (x 14),  $NO_3^-$  (x 45) and  $Br^-$  (x 50) at the same normality of  $Na^+$ . The univalent anions, especially large-volume anions such as  $NO_3^-$  and  $Br^-$  exhibit better emission enhancement than divalent anions. It is noteworthy that  $Br^-$  causes 50 times of fluorescence enhancement of  $OF_1^+$ , which is higher than  $Cl^-$  and even has the highest sensitivity to fluorescence than all other anions.

The similar experiments about ion effect of different chloride salts are studied. The emission spectra of organic quaternary aminated  $OF_1^+$  in aqueous solution of different chloride salts are also investigated (Fig. 3). As shown in Figure 3a-3e, the blue emission of  $OF_1^+$  in water decreases significantly while their yellow emission increases abruptly along with ion concentration increasing. The emission enhancement of  $OF_1^+$  is similar, i.e.,  $Na^+$  (x 14),  $Ca^{2+}$  (x 15),  $Mg^{2+}$  (x16),  $K^+$  (x 16) and  $NH_4^+$  (x 17). There is no much difference due to ion concentration effect of different cations,

which may be attributed to the less extent of interaction between the identical electrical charges of salt cations and cationic oligoelectrolyte  $OF_1^+$ .

In the molecular structure of  $OF_n^+$  ( $n = 1-3$ ), the 9-C position of each fluorene is replaced by a pair of six-carbon hydrophobic alkyl chains containing positively charged, quaternary ammonium head groups which will interact with anionic cell membrane, intercalate into the cell membrane and increase the membrane permeability by distorting the arrangement of membrane phospholipids.  $OF_n^+$  ( $n = 1-3$ ) are assessed for their ability to localize and stain subcellular structures in living cells by fluorescence microscope. Cervical cancer HeLa cells are incubated with 5  $\mu M$   $OF_n^+$  ( $n = 1-3$ ) for 2 h, followed by 50 nM LysoTracker Red (a commercial probe for Lysosomes) for another 45 mins.  $OF_n^+$  ( $n = 1-3$ ) staining the HeLa cells (Fig. 4a, 4e and 4i) overlaps well with the containing LysoTracker Red (Fig. 4b, 4f and 4j). The Pearson's correlation coefficients between the green-yellow emissions from  $OF_n^+$  ( $n = 1-3$ ) and the red emissions from LysoTracker Red were determined to be 92.9% ( $OF_1^+$ ), 90.1% ( $OF_2^+$ ) and 68.7% ( $OF_3^+$ ), respectively, demonstrating the specific targeting of  $OF_n^+$  ( $n = 1-2$ ) to lysosomes. Compared with  $OF_3^+$ , both  $OF_1^+$  and  $OF_2^+$  show better imaging results, which may be attributed to the smaller molecular scale and higher lipophilicity of them. The colocalization experiment of  $OF_n^+$  ( $n = 1-3$ ) with MitoTracker Red (A commercial probe for mitochondria) was also carried out (Fig. S6). The blue signal of  $OF_n^+$  ( $n = 1-3$ ) overlaps poor with the red signal of MitoTracker Red. These experiment results indicate that  $OF_n^+$  ( $n = 1-3$ ) with high cell membrane permeability could specifically target lysosomes. The cells still have a good morphology and life activity which can be seen

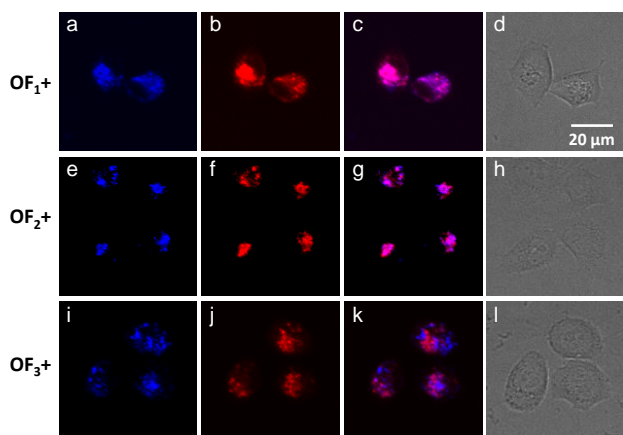


**Fig. 4** Confocal images of HeLa cells stained with 5.0  $\mu\text{M}$   $\text{OF}_n^+$  and 50 nM LysoTracker Red. The 1st column: distribution of  $\text{OF}_n^+$  on Channel 1 ( $\lambda_{\text{ex}} = 405$  nm,  $\lambda_{\text{em}} = 415\text{-}475$  nm); The 2nd column: distribution of LysoTracker Red on Channel 2 ( $\lambda_{\text{ex}} = 561$  nm,  $\lambda_{\text{em}} = 580\text{-}650$  nm). The 3rd column: the Merged image of 2nd and 3rd columns; The 4th column: bright-field image. Scale bar = 20  $\mu\text{m}$ .

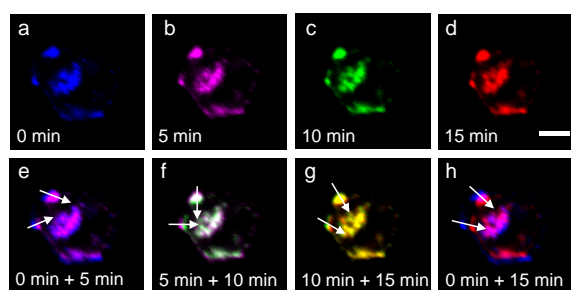


**Fig. 5** Confocal images of a HeLa cell stained with 5.0  $\mu\text{M}$   $\text{OF}_1^+$  and stimulated using 5  $\mu\text{M}$  chloroquine. Different pseudocolors are used to display the fluorescence images at different stimulation times: (a) 0 min, (b) 5 min, (c) 10 min, (d) 15 min; Merged images at two different moments: (e) 0 min and 5 min, (f) 5 min and 10 min, (g) 10 min and 15 min and (h) 0 min and 15 min. The white arrows in (e)-(h) are used to trace the movement direction of lysosome. Scale bar = 5  $\mu\text{m}$ .

from the bright field (Fig. 4d, 4h and 4l). This indicates a relatively low cytotoxicity of  $\text{OF}_n^+$  ( $n = 1\text{-}3$ ).

As the spatial and temporal distribution of lysosomes can also help to diagnose the lysosomal storage diseases or tracking lysosomal movements (Fig. 5). The cells are stimulated using 5.0  $\mu\text{M}$  of chloroquine, which can drive lysosomal migration without inducing any other apparent disturbance in the cells.<sup>19</sup> The movement of lysosomes is subsequently monitored by confocal microscopy. As shown in Fig. 5, the slight movement could be observed in Fig. 5a-5d and unambiguously traced in the merged images (Fig. 5e-5h) at any time interval. Such a good image quality of  $\text{OF}_1^+$  for tracing lysosomes should be ascribed to the superior fluorescence photostability of  $\text{OF}_1^+$  independent of pH environment within lysosomes.

In conclusion, by means of GCC, we have designed and synthesized two series of xanthene-contained AIE luminesgens, hydrophobic neutral conjugated tetraarylethene  $\text{OF}_n$  ( $n = 1\text{-}3$ ) and corresponding hydrophilic cationic conjugated oligoelectrolytes  $\text{OF}_n^+$  ( $n = 1\text{-}3$ ) with aggregating-induced emission activity. Both  $\text{OF}_n$  ( $n = 1\text{-}3$ ) and  $\text{OF}_n^+$  ( $n = 1\text{-}3$ ) exhibit synergistical ratiometric aggregation-induced emission (AIE)

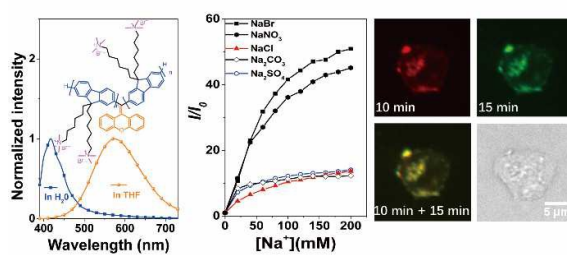
(peaked at around 550 nm) and aggregation-induced quenching (ACQ) characteristics (peaked at around 420 nm), which significantly increase the ratiometric fluorescence contrast above 2000.  $\text{OF}_n^+$  ( $n = 1\text{-}3$ ) exhibit excellent ion-induced emission in aqueous solution, in which monovalent ions show better fluorescence enhancement than divalent ions.  $\text{OF}_n^+$  ( $n = 1\text{-}2$ ) exhibit excellent colocalization to lysosomes of living HeLa cells, which are also used for fluorescence imaging and tracing of lysosome events.

This work was supported by the National Basic Research Program (973) of China (2015CB755602 and 2013CB922104), the Natural Science Foundation of China (51673077, 21474034 and 51603078) and the Fundamental Research Funds for the Central Universities (HUST: 2016YXMS029). We also thank to the facility support of the Analytical & Testing Center of Huazhong University of Science & Technology, the Center of Micro-Fabrication & Characterization (CMFC) and the Center for Nanoscale Characterization & Devices (CNCD) of WNLO.

## Notes and references

- J. Luo, Z. Xie, J. W. Y. Lam, L. Cheng, H. Chen, C. Qiu, H. S. Kwok, X. Zhan, Y. Liu, D. Zhu, B. Z. Tang, *Chem. Commun.*, 2001, 1740-1741.
- J. Mei, N. L. C. Leung, R. T. K. Kwok, J. W. Y. Lam and B. Z. Tang, *Chem. Rev.*, 2015, **115**, 11718-11940.
- N. Zhao, Z. Yang, J. W. Y. Lam, H. H. Y. Sung, N. Xie, S. Chen, H. Su, M. Gao, I. D. Williams, K. S. Wong and B. Z. Tang, *Chem. Commun.*, 2012, **48**, 8637-8639.
- J. Huang, N. Sun, P. Chen, R. Tang, Q. Li, D. Ma and Z. Li, *Chem. Commun.*, 2014, **50**, 2136-2138.
- G.-F. Zhang, M. P. Aldred, W.-L. Gong, C. Li and M.-Q. Zhu, *Chem. Commun.*, 2012, **48**, 7711-7713.
- L. Yan, Y. Zhang, B. Xu and W. Tian, *Nanoscale*, 2016, **8**, 2471-2487.
- Y. Yuan, W. Wu, S. Xu and B. Liu, *Chem. Commun.*, 2017, **53**, 5287-5290.
- C. Li and S. Liu, *Chem. Commun.*, 2012, **48**, 3262-3278.
- C. Chen, Z. Song, X. Zheng, Z. He, B. Liu, X. Huang, D. Kong, D. Ding and B. Z. Tang, *Chem. Sci.*, 2017, **8**, 2191-2198.
- X. Y. Shen, Y. J. Wang, H. Zhang, A. Qin, J. Z. Sun and B. Z. Tang, *Chem. Commun.*, 2014, **50**, 8747-8750.
- Z. Zhao, J. W. Y. Lam and B. Z. Tang, *J. Mater. Chem.*, 2012, **22**, 23726-23740.
- N.-H. Xie, C. Li, J.-X. Liu, W.-L. Gong, B.-Z. Tang, G. Li and M.-Q. Zhu, *Chem. Commun.*, 2016, **52**, 5808-5811.
- M. P. Aldred, C. Li, G.-F. Zhang, W.-L. Gong, A. D. Q. Li, Y. Dai, D. Ma and M.-Q. Zhu, *J. Mater. Chem.*, 2012, **22**, 7515-7528.
- Z.-Q. Chen, T. Chen, J. X. Liu, G. F. Zhang, C. Li, W.-L. Gong, Z. J. Xiong, N.-H. Xie, B. Z. Tang and M.-Q. Zhu, *Macromolecules*, 2015, **48**, 7823-7831.
- R. Hu, N. L. C. Leung and B. Z. Tang, *Chem. Soc. Rev.*, 2014, **43**, 4494 - 4562.
- G.-F. Zhang, H. Wang, M. P. Aldred, T. Chen, Z.-Q. Chen, X. Meng and M.-Q. Zhu, *Chem. Mater.*, 2014, **26**, 4433-4446.
- J. Shi, N. Chang, C. Li, J. Mei, C. Deng, X. Luo, Z. Liu, Z. Bo, Y. Q. Dong and B. Z. Tang, *Chem. Commun.*, 2012, **48**, 10675-10677.
- Y. Honmou, S. Hirata, H. Komiyama, J. Hiyoshi, S. Kawauchi, T. Iyoda and M. Vacha, *Nat. Commun.*, 2014, **5**, 4666.
- Y. Cai, C. Gui, K. Samedov, H. Su, X. Gu, S. Li, W. Luo, H. H. Y. Sung, J. W. Y. Lam, R. T. K. Kwok, I. D. Williams, A. Qin and B. Z. Tang, *Chem. Sci.*, 2017, **8**, 7593-7603.

## Table of contents entry



Novel ratiometric AIE-active tetraarylethene oligoelectrolytes synthesized by Geminal cross-coupling show ion-induced emission and are applied as bioprobes for lysosome tracing.